Science World Journal Vol. 21(No 2) 2026 https://dx.doi.org/10.4314/swj.v21i2.23
www.scienceworldjournal.org
ISSN: 1597-6343 (Online), ISSN: 2756-391X (Print)
Published by Faculty of Science, Kaduna State University

Full Length Research Article

STRUCTURAL CONTROL AND GEOCHEMICAL EVOLUTION OF Pb-Zn-Cu MINERALIZATION: A MULTIVARIATE STATISTICAL APPROACH USING CENTRED LOG-RATIO (CLR) TRANSFORMATION AND PRINCIPAL COMPONENTS ANALYSIS

*[1,2]Ayodeji Enoch Olorunyomi, [2]Samuel Bamidele Olobaniyi, [2]Abiodun Mary Odukoya, [1]Ifeoma Aquila Ekeleme

[1]Department of Geology, University of Jos, Jos, Plateau State, Nigeria
[2]Department of Geosciences, University of Lagos, Akoka, Lagos State, Nigeria.

*Corresponding Author Email Address: olorunyomia@unijos.edu.ng

ABSTRACT
The Saiya-Shokobo and Tongolo alkaline ring complexes of North-Central Nigeria host significant Pb-Zn-Cu mineralization. However, the structural controls and paragenetic evolution of these deposits remain poorly understood. This study integrates detailed structural mapping with Compositional Data Analysis (CoDA), employing the Centred Log-Ratio (CLR) transformation and Principal Component Analysis (PCA) of lithogeochemical data to distinguish discrete mineralization events within the Younger Granite and basement rock units. Structural analysis identifies dominant NNE-SSW, NNW-SSE, NE-SW, and N-S trends, indicating that reactivated Pan-African shear zones acted as major conduits for hydrothermal fluids. CLR-PCA further demonstrates that mineralization-related signatures are concentrated in lower-eigenvalue components beyond the lithological background represented by PC1–PC3. In the Younger Granites, PC5 (λ = 0.66) defines a Cu-Pb association interpreted as evidence of telescoped hydrothermal activity involving successive high- and low-temperature fluid pulses. In contrast, PC4 (λ = 0.60) within the basement rocks is characterized by a distinct Pb signature, suggesting pre-magmatic metal enrichment. These findings support a dual-source metallogenic model in which the Nigerian basement served as a pre-enriched metal reservoir, subsequently overprinted by magmatic-hydrothermal fluids associated with the anorogenic Younger Granite event. The study demonstrates the effectiveness of CoDA-based multivariate analysis for resolving previously unresolved paragenetic stages in polymetallic hydrothermal systems.

Keywords: Centred log-ratio transformation, Principal component analysis, Pb-Zn-Cu mineralization, Lithogeochemistry, Nigerian Younger Granites

INTRODUCTION

Polymetallic deposits, including those rich in lead (Pb), zinc (Zn), and copper (Cu), represent significant economic resources globally; they are commonly found within or near granitic rocks and granitoids. These deposits typically form via magmatic – hydrothermal processes, where cooling, highly differentiated granitic magmas release ore – bearing fluids (Bestemianova & Grinev, 2019; Yan *et al*., 2024; Du *et al*., 2025; Li *et al.*, 2024; Bailie & Robb, 2004; Yang *et al.,* 2025). Traditional univariate statistical methods for geochemical anomaly detection fail to account for the multivariate nature and compositional constraints of lithogeochemical data, leading to spurious correlations due to the constant-sum problem. To overcome these challenges, compositional data analysis (CoDA) techniques, such as log-ratio transformations, have been developed to open the data simplex and enable meaningful statistical interpretation (Aitchison, 1986; Egozcue *et al*., 2003; Filzmoser *et al*., 2009; Filzmoser *et al*., 2010; Reimann *et al*., 2017). The centred log-ratio (CLR) transformation, in particular, preserves relative information among components and is suitable for multivariate methods such as principal components analysis (PCA), which reduces dimensionality while highlighting elemental associations indicative of mineralization. Recent applications have demonstrated the efficacy of CLR-PCA in identifying geochemical anomalies in polymetallic systems, including Pb-Zn-Cu skarns and vein deposits (Reimann *et al.,* 2012; Zuo, 2011; Zuo *et al.,* 2013; Wang *et al.,* 2021; Wang *et al.,* 2024; Seyedrahimi-Niaraq *et al*., 2025).

In previous work, we characterized the petrographic features of potential host rocks and identified ore minerals to understand the controls on mineralization. We observed that galena, sphalerite, chalcopyrite, and pyrite are hosted in rhyolites, porphyritic granites, pegmatitic granite gneisses, and migmatites in the study area (Olorunyomi *et al.,* in press). Building on these findings, the current study investigates the structural controls and geochemical evolution of Pb-Zn-Cu mineralization using a multivariate statistical approach based on CLR and PCA, applied to lithogeochemical data from the Saiya – Shokobo and Tongolo Younger Granites Complexes of the Nigerian Younger Granites (NYG) province as a case study. The peculiarities of the data, such as skewed distributions, high variance in trace elements, and elemental associations, are incorporated to elucidate mineralization patterns. The study aims to reveal geochemical anomalies and mineralization, interpret genetic implications, and provide a template for similar rocks within the Nigerian Younger Granites province.

Geological Setting

The study area is situated between latitudes 10°18'30" N and 10°30'00" N and longitudes 8°58'00" E and 9°09'30" E, covering parts of Lere Sheet 147 NE and Toro Sheet 148 NW, Nigeria. The

Science World Journal Vol. 21(No 2) 2026 https://dx.doi.org/10.4314/swj.v21i2.23
www.scienceworldjournal.org
ISSN: 1597-6343 (Online), ISSN: 2756-391X (Print)
Published by Faculty of Science, Kaduna State University

area is underlain by Basement Complex rocks, which have been intruded by the Saiya – Shokobo and Tongolo Younger Granites Complexes (Fig.1). The Complexes consist of dolerites, gabbros, syenites, agglomerates, ignimbrites, basalts, granites, and rhyolites. The intruded basement consists of the Migmatite-Gneiss complex, Pan-African granitoids, acid and basic dykes. Structural trends in the Younger Granites suggest that deep-seated basement structures controlled them. These structures provided channels not only for the rise of magma but also for the movement of ore-rich hydrothermal fluids. These structures have been reactivated at different times throughout the Phanerozoic and dictated the location of the alkaline igneous complexes and their mineralization (Imeokparia, 1985; Kinnaird & Bowden, 1987; Solomon, 2005; Obaje, 2009; Aga & Haruna, 2019).

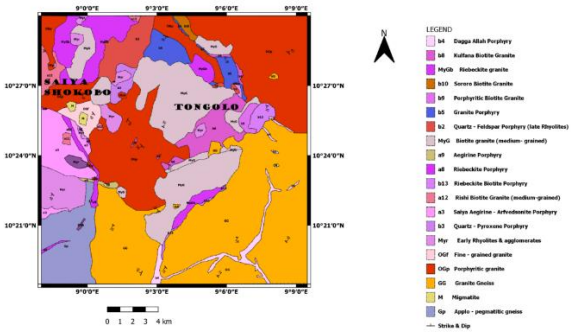

Figure 1. Geological map of the study area (modified after (Kinnaird & Bowden, 1987; Imeokparia, 1985**)**

MATERIALS AND METHODS

Data collection and analysis

Lithogeochemical samples were collected from the rocks in the study area. We employed a random sampling strategy to obtain a representative suite of rocks and ore materials from the identified lithological units. This also helped to minimize bias and ensure that all lithological units had an equal probability of being sampled. A total of forty samples were selected for analysis. These samples were crushed using a jaw crusher and pulverized to a fine powder (<75 µm) using an agate mortar at the geochemical laboratory of the Department of Geology, University of Jos, Nigeria. Ten (10) grams of each pulverized sample were stored in small polythene bags and transported to the geochemical laboratory of the Lagos State Environmental Protection Agency (LASEPA), Nigeria, for digestion and analysis. Samples were digested using a multi-acid mixture of HF + HNO_3 + $HClO_4$, following established protocols for geological matrices (Etschmann et al., 2019; Watts et al., 2019). Digested solutions were analysed for major and trace elements using the Agilent 4200 Microwave Plasma-Atomic Emission Spectroscopy (MP-AES) instrument.

The data exhibited positive skewness and closure effects, typical of compositional datasets. Trace elements data are presented in this paper (Tables 1,2,3). Elemental subcompositions associated with, and are suitable pathfinders for Pb, Zn, and Cu mineralization, namely Pb, Zn, Cu, Cd, As, Ba, Fe, and Mn, were selected for further statistical analysis. This approach is fundamental to modern geochemical studies (Darabi-Golestan & Hezarkhani, 2019; Du *et al.,* 2025; Erlandsson *et al.,* 2025).

Geochemical Data Toolkit (GCDkit) software (version 6.2.0) was used to perform the Centered log-ratio transformation of the raw data (Tables 4, 5, 6, 7). Principal Component Analysis (PCA), biplots (Fig. 2, Fig. 3), PC loadings, eigenvalues, variance, and scores were obtained using the R program (version 4.1.3) and tabulated (Tables 8, 9). Geochemical maps were generated using Surfer software (Version 13.4.553) to visualize anomaly thresholds based on PC scores. Structural features within the major lithologies were observed, analysed and compared to the major lineaments in the study area.

Centred Log-Ratio Transformation

To address the closure problem, the lithogeochemical data (Tables 1,2,3) were transformed using the CLR method (Aitchison, 1986), defined as:

$\mathrm{Clr}(x_i) = \ln\left(\frac{xi}{g(x)}\right)$

Where x_i is the i-th component, and $g(x)$ is the geometric mean of all components. This transformation (Tables 4, 5, 6, 7) opens the data, allowing for standard statistical procedures without spurious correlations (Egozcue *et al*., 2003).

Principal Components Analysis

PCA was applied to the CLR-transformed data to extract principal components (PCs) explaining the variance. The number of PCs was determined by eigenvalues >1 (Jolliffe, 2002; Jolliffe & Cadima, 2016). Biplots (Fig.2, Fig.3) and loading matrices (Tables 8, 9) identified elemental associations. Lower principal components (PC1, PC2) typically capture large-scale lithological variations or the dominant background. In contrast, higher principal components (e.g., PC4, PC5) with exploration potential or mineralization signals, which are often subtler, explain less variance (Grunsky et al., 1999; Grunsky et al., 2014; Grunsky et al., 2020).

transformation (CLR), Principal Components Analysis (PCA) data, and biplots are presented in the tables and figures below;

RESULTS

The trace elements concentration, Centred log-ratios

Table 1a. Trace element data for the Saiya – Shokobo Complex

COMPLEX	SAIYA-SHOKOBO											
SAMPLE I.D	D1a	D1b	D1c	D12	D18	S1a	S1c	S2a	S2b	S6	S15b	S17b
LOCATION NAME	DAWA	DAWA	DAWA	DAWA	DAWA	DAWA	DAWA	DAWA	DAWA	DAWA	DAWA	DAWA
ROCK TYPE	medium grained biotite Granite	Rhyolite	Rhyolite	Rhyolite	medium-grained biotite Granite	medium-grained biotite Granite	Rhyolite (Ore material)	Medium-grained granite (Saiya porphyry)	Granite (Ore material)	Rishi biotite Granite	medium-grained Granite	Fine-grained biotite-muscovite granite

Science World Journal Vol. 21(No 2) 2026 https://dx.doi.org/10.4314/swj.v21i2.23
www.scienceworldjournal.org
ISSN: 1597-6343 (Online), ISSN: 2756-391X (Print)
Published by Faculty of Science, Kaduna State University

					e							
LATITU	10.4	10.4	10.4	10.4	10.4	10.4	10.43	10.4272	10.42	10.4	10.47	10.4321
LONGI	8.98	8.98	8.98	8.99	8.99	8.98	8.984	8.9822	8.982	8.98	8.997	9.0023
As	129.	47.7	57.4	57.2	21.6	0.01	97.12	130.284	39.74	33.1	0.015	67.967
B	3.66	4.86	0.01	3.17	0.01	3.65	0.015	3.835	2.227	0.01	1.989	0.423
Ba	130.	119.	76.6	817.	65.8	562.	319.4	154.590	38.31	175.	45.69	140.383
Be	3.24	5.55	8.15	3.39	6.19	4.85	3.912	4.182	4.404	9.83	4.746	3.623
Cd	2.99	2.61	390.	3.90	104.	9.69	3.994	4.151	7.164	5.21	7.239	2.944
Co	6.56	1.14	0.01	0.01	0.01	0.01	0.015	4.958	0.015	0.01	0.015	0.015
Cr	5.05	6.16	5.46	4.98	4.75	4.80	4.757	17.291	5.784	6.55	8.404	4.777
Cu	10.4	19.6	122.	13.9	365.	13.8	11.86	21.232	20.13	92.2	14.07	40.567
Ga	55.5	52.4	125.	58.2	154.	33.9	61.99	68.092	57.71	147.	59.25	64.175
In	858.	806.	1124	886.	1158	653.	923.5	1079.747	1012.	949.	994.9	758.406
Li	27.2	16.9	2664	268.	213.	21.8	4.569	18.960	18.73	597	4.361	13.705
Ni	12.1	12.5	1.36	12.4	4.34	0.01	12.76	18.485	13.81	6.48	7.218	11.486
Pb	131.	234.	154.	82.6	9548	86.8	92.89	90.910	365.7	100.	118.8	109.513
Sc	0.05	0.05	0.05	0.05	0.05	0.05	0.050	0.050	0.050	0.05	0.050	0.050
Se	912.	629.	751.	694.	398.	100.	734.8	945.645	703.0	789.	438.5	578.522
Th	7.59	3.45	0.00	1.54	0.00	9.32	0.001	6.037	0.001	0.00	0.949	0.001
U	173.	169.	246.	167.	240.	138.	162.1	204.763	204.8	198.	160.2	118.884
V	6.98	13.4	9.30	8.71	38.1	7.68	12.18	36.375	7.623	2.27	9.631	10.569
Zn	319.548	839.848	1505 0.53	327.032	7542 .758	413.431	342.1 86	163.937	652.6 00	117 5.57	905.2 04	221.616

Table 1b. Trace element data for the Saiya – Shokobo Complex (continued)

COMPLEX	**SAIYA-SHOKOBO**						
SAMPLE I.D	**S7**	**S18**	**S19**	**S20a**	**S21a**	**S22b**	**S24c**
LOCATION NAME	**ZALAU _1**	**RIGA**	**RIGA**	**RIGA**	**RIGA**	**RIGA**	**RIGA**
ROCK TYPE	**Rhyolite**	**medium-grained Granite**	**medium-grained Granite**	**Rhyolite**	**Rhyolite**	**Quartz - feldspar porphyry**	**Rhyolite (Ore material)**
LATITUDE	10.3855	10.4322	10.4389	10.4525	10.4539	10.4544	10.4654
LONGITUDE	8.9986	9.0079	9.0117	9.0125	9.0111	9.0178	9.0400
As (ppm)	97.443	152.789	129.334	112.547	88.095	64.675	0.015
B	0.327	3.356	3.491	2.950	3.698	0.015	1.670
Ba	269.287	40.161	57.108	44.692	21.715	61.429	62.831
Be	4.264	5.808	4.781	4.838	3.306	6.374	8.375
Cd	6.304	3.041	3.365	2.977	3.538	146.282	12.456
Co	0.015	2.171	7.243	1.327	3.980	0.015	0.015
Cr	7.102	7.284	7.046	6.395	4.599	6.070	5.561
Cu	20.158	12.714	89.424	13.123	12.108	119.538	15.752
Ga	79.327	77.184	69.118	74.988	55.536	132.834	54.678
In	1139.510	1130.168	1096.037	1049.976	782.851	1066.809	1039.332
Li	8.572	579.663	5.090	294.075	236.338	2792.967	215.543
Ni	17.609	11.857	17.351	14.370	10.602	10.531	0.015
Pb	144.323	89.516	119.140	172.835	82.500	164.997	147.133
Sc	0.050	0.050	0.050	0.050	0.050	0.050	0.050
Se	945.818	1174.249	955.889	885.288	705.398	673.190	73.089
Th	0.001	4.114	0.001	4.807	7.884	0.001	3.300
U	202.571	207.234	197.087	210.957	151.176	214.437	187.931
V	20.444	12.342	13.536	10.315	8.267	3.315	10.565
Zn	589.919	373.438	406.907	785.721	799.229	9980.170	745.803

Science World Journal Vol. 21(No 2) 2026 https://dx.doi.org/10.4314/swj.v21i2.23
www.scienceworldjournal.org
ISSN: 1597-6343 (Online), ISSN: 2756-391X (Print)
Published by Faculty of Science, Kaduna State University

Table 2. Trace element data for the Tongolo Complex

COMPLEX	TONGOLO									
SAMPLE I.D	K1	S10	S11	S12	P10a	P18b	S13a	S26c	S29a	S30
LOCATION NAME	KULFANA	KULFANA	KULFANA	KULFANA	MANA	MANA	PAKURU	DAGGA ALLAH	DAGGA ALLAH	DAGGA ALLAH
ROCK TYPE	Fine - medium-grained biotite Granite	Kulfana biotite Granite	Biotite Granite	Hornblende - biotite Granite	medium-grained biotite Granite	Biotite Granite	Rhyolite	Granite (Ore material)	Porphyritic Rhyolite	medium-grained Granite
LATITUDE	10.4234	10.4092	10.4315	10.4624	10.3765	10.3773	10.4901	10.3195	10.3256	10.3290
LONGITUDE	9.0882	9.0666	9.0687	9.0770	9.0966	9.0975	9.0926	9.1131	9.0980	9.0964
As (ppm)	84.051	89.375	0.015	167.296	0.015	76.762	4.955	122.786	82.943	31.827
B	2.091	0.015	1.947	3.840	0.015	1.471	0.015	0.063	0.015	0.015
Ba	163.244	205.483	80.807	83.332	60.982	53.685	97.843	34.546	59.068	511.255
Be	5.142	4.296	5.563	5.138	100.695	12.087	6.134	3.734	5.623	6.341
Cd	6.170	2.318	8.866	2.715	14.685	4.771	14.692	6.951	3.931	72.820
Co	0.145	0.015	0.015	2.153	0.015	0.015	0.015	0.015	0.015	0.015
Cr	0.601	4.056	4.831	5.723	4.008	6.835	5.073	4.628	4.997	6.458
Cu	18.134	13.693	11.322	17.338	15.449	16.298	15.819	10.633	19.074	43.387
Ga	104.937	81.367	34.652	78.581	58.294	86.344	94.767	66.057	67.141	86.113
In	1002.702	1002.144	631.881	1130.304	966.184	1137.756	909.184	795.264	1088.926	915.018
Li	29.868	38.259	220.309	107.371	61.477	14.341	345.970	481.626	11.599	1958.543
Ni	15.739	11.478	0.015	13.316	0.015	16.214	3.656	8.599	13.776	8.093
Pb	125.895	83.700	72.652	222.003	87.336	121.856	109.127	91.217	154.963	208.828
Sc	0.050	3.137	0.050	0.050	0.050	0.050	0.050	0.050	0.050	0.050
Se	816.536	889.775	146.815	1112.692	0.003	909.965	353.690	760.823	979.470	639.116
Th	0.001	4.730	0.073	7.489	0.001	0.001	0.001	5.947	5.350	0.001
U	96.241	146.895	122.013	190.936	200.222	210.871	318.777	155.064	199.074	159.974
V	1.998	35.504	5.805	10.112	4.092	11.920	2.405	6.915	11.025	21.993
Zn	426.484	195.125	224.026	688.829	2044.939	609.758	2507.290	1578.046	647.979	6349.938

Table 3. Trace element data for the basement rocks

COMPLEX	BASEMENT										
SAMPLE I.D	D2b	D24a	D25a	S16	K14	K22	S13c	S14	S26b	S28	S29c
LOCATION NAME	DAWA		DAWA		KULFANA	ZALAU_2	PAKURU		DAGGA ALLAH	DAGGA ALLAH	DAGGA ALLAH
ROCK TYPE	Migmatite (ore material)	Migmatite	Migmatite (ore material)	Granite Gneiss	Porphyritic Granite	Porphyritic Granite	Porphyritic Granite	Porphyritic Granites (Ore material)	Granite Gneiss	Dolerite	Porphyritic Granite
LATITUDE	10.4246	10.4284	10.4248	10.4450	10.3885	10.4073	10.4901	10.4721	10.3195	10.3184	10.3256

Science World Journal Vol. 21(No 2) 2026 https://dx.doi.org/10.4314/swj.v21i2.23
www.scienceworldjournal.org
ISSN: 1597-6343 (Online), ISSN: 2756-391X (Print)
Published by Faculty of Science, Kaduna State University

LONGITUDE	8.9969	8.9956	8.9969	8.9781	9.0505	9.0543	9.0926	9.1092	9.1131	9.1019	9.0980
As (ppm)	141.650	334.230	0.015	103.225	0.015	0.015	150.254	60.645	96.694	0.015	32.708
B	1.368	0.302	0.015	0.015	0.015	0.015	5.297	3.179	1.434	0.015	0.015
Ba	15.111	4.694	92.044	758.428	517.046	1841.562	13.737	45.195	753.985	260.412	63.495
Be	6.316	2.828	8.766	6.187	4.961	11.756	3.441	4.687	4.089	5.362	5.885
Cd	5.886	5.512	355.197	8.347	5.088	12.150	3.168	3.273	62.258	9.512	10.343
Co	1.776	31.318	0.015	0.015	0.015	0.015	16.335	3.286	6.329	0.015	0.015
Cr	14.687	6.955	8.850	5.330	32.712	504.300	6.769	5.478	6.450	3.636	5.654
Cu	19.516	7.624	143.956	26.342	16.061	132.525	10.620	13.287	20498.732	10.565	47.250
Ga	59.932	45.697	198.521	109.665	67.254	109.215	60.222	55.150	66.559	44.385	90.747
In	894.117	70.627	871.540	1241.086	913.196	1295.171	993.714	873.999	712.374	722.637	1192.125
Li	8.958	3.716	8400.483	95.474	72.849	287.523	3.545	37.070	104.693	197.610	1079.314
Ni	9.585	19.576	0.015	12.281	13.201	56.503	24.927	13.314	9.535	0.015	11.837
Pb	117.301	25.639	145.432	135.594	89.252	133.494	80.475	91.310	277.112	204.413	324.182
Sc	0.050	0.050	0.050	1.132	6.469	19.025	0.050	0.050	0.599	0.050	0.050
Se	908.210	1036.321	620.486	955.759	455.419	70.089	1166.429	747.686	804.496	0.003	681.298
Th	0.832	21.122	0.001	0.001	0.001	0.001	10.828	0.001	6.996	0.001	0.001
U	181.021	96.011	229.987	204.776	149.481	218.976	206.497	168.610	190.100	120.031	194.736
V	7.978	10.648	4.478	29.858	129.472	594.223	11.292	8.809	21.230	4.203	8.948
Zn	546.086	693.469	12253.389	716.132	441.653	548.724	154.651	398.028	8537.898	503.672	1458.775

Table 4. Centered log-ratio transformation of trace elements data of the Saiya – Shokobo and Tongolo Complexes

	Pb_clr	Zn_clr	Cu_clr	Li_clr	As_clr	B_clr	Ba_clr	Be_clr	Cd_clr	Co_clr	Cr_clr	Ga_clr	In_clr	Ni_clr	Sc_clr	Se_clr	Th_clr	U_clr	V_clr
S1	2.23	3.12	-0.30	0.65	2.21	-1.35	2.22	-1.47	-1.55	-0.77	-1.03	1.37	4.10	-0.16	-5.65	4.16	-0.62	-2.51	-0.71
S2	2.88	4.15	0.40	0.25	1.28	-1.00	2.20	-0.87	-1.62	-2.44	-0.76	1.38	4.11	-0.06	-5.58	3.86	-1.34	-2.55	0.02
S3	3.33	7.91	3.10	6.18	2.34	-5.91	2.63	0.39	4.26	-5.91	-0.02	3.12	5.31	-1.40	-4.71	4.91	-8.62	-3.79	0.52
S4	1.96	3.33	0.18	3.13	1.59	-1.30	4.25	-1.24	-1.10	-6.66	-0.85	1.61	4.33	0.06	-5.46	4.08	-2.03	-2.66	-0.29
S5	7.40	7.17	4.14	3.60	1.31	-5.96	2.43	0.06	2.89	-5.96	-0.20	3.28	5.29	-0.29	-4.76	4.23	-8.67	-3.72	1.88
S6	2.75	4.31	0.91	1.37	-5.91	-0.42	4.62	-0.13	0.56	-5.91	-0.14	1.81	4.77	-5.91	-4.71	2.89	0.52	-3.22	0.33
S7	2.72	4.02	0.66	-0.29	2.76	-6.01	3.95	-0.45	-0.43	-6.01	-0.25	2.31	5.02	0.73	-4.81	4.79	-8.72	-3.28	0.69
S8	1.70	2.29	0.24	0.13	2.06	-1.47	2.23	-1.38	-1.39	-1.21	0.04	1.41	4.17	0.10	-5.81	4.04	-1.01	-2.51	0.78
S9	3.86	4.44	0.96	0.89	1.64	-1.24	1.60	-0.56	-0.08	-6.24	-0.29	2.01	4.88	0.58	-5.04	4.51	-8.95	-3.28	-0.01
S10	3.14	5.60	3.06	7.23	2.03	-5.67	3.70	0.82	0.18	-5.67	0.41	3.52	5.39	0.40	-4.46	5.20	-8.38	-3.82	0.65
S11	2.71	4.74	0.58	-0.59	-6.27	-1.31	1.75	-0.51	-0.09	-6.27	0.06	2.01	4.84	-0.09	-5.06	4.02	-2.12	-3.01	0.20

Science World Journal Vol. 21(No 2) 2026 https://dx.doi.org/10.4314/swj.v21i2.23
www.scienceworldjournal.org
ISSN: 1597-6343 (Online), ISSN: 2756-391X (Print)
Published by Faculty of Science, Kaduna State University

S12	2.60	3.31	1.61	0.52	2.13	-8 -2.95	2.85	-0.81	-1.01	-6.29	-0.53	2.07	4.54	0.35	-5.09	4.27	-9.00	2.68	0.26
S13	2.68	4.09	0.71	-0.14	2.29	-3.41	3.31	-0.84	-0.45	-6.49	-0.33	2.08	4.75	0.58	-5.29	4.56	-9.20	3.02	0.73
S14	1.73	3.16	-0.22	3.60	2.26	-1.55	0.93	-1.01	-1.65	-1.99	-0.78	1.58	4.26	-0.29	-5.76	4.30	-1.35	2.57	-0.25
S15	2.36	3.59	2.08	-0.79	2.44	-1.17	1.63	-0.85	-1.20	-0.44	-0.47	1.82	4.58	0.44	-5.41	4.44	-9.33	2.87	0.19
S16	2.40	3.91	-0.18	2.93	1.97	-1.67	1.05	-1.18	-1.66	-2.47	-0.90	1.56	4.20	-0.09	-5.75	4.03	-1.18	2.60	-0.42
S17	1.80	4.07	-0.12	2.85	1.86	-1.31	0.46	-1.42	-1.35	-1.24	-1.09	1.40	4.05	-0.26	-5.61	3.94	-0.55	2.40	-0.50
S18	3.37	7.47	3.04	6.20	2.43	-5.94	2.38	0.11	3.25	-5.94	0.06	3.15	5.23	0.61	-4.74	4.77	-8.65	3.63	0.54
S19	3.20	4.82	0.96	3.58	-6.00	-1.28	2.34	0.33	0.73	-6.00	-0.08	2.21	5.15	-6.00	-4.79	2.50	-0.60	3.44	0.56
T1	2.36	3.58	0.42	0.92	1.95	-1.74	2.62	-0.84	-0.66	-4.41	-2.99	2.18	4.43	0.28	-5.47	4.23	-9.39	2.09	-1.79
T2	1.87	2.72	0.06	1.09	1.94	-6.75	2.77	-1.10	-1.71	-6.75	-1.15	1.84	4.36	-0.11	-1.41	4.24	-1.00	2.44	1.02
T3	2.66	3.78	0.80	3.77	-5.83	-0.96	2.76	0.09	0.55	-5.83	-0.05	1.92	4.82	-5.83	-4.62	3.36	-4.25	3.18	0.13
T4	2.32	3.45	-0.23	1.59	2.03	-1.74	1.34	-1.45	-2.09	-2.32	-1.34	1.28	3.94	-0.50	-6.08	3.93	-1.07	2.17	-0.77
T5	4.31	7.46	2.57	3.96	-4.36	-4.36	3.95	4.45	2.52	-4.36	1.23	3.90	6.71	-4.36	-3.16	-5.97	-7.07	5.14	1.25
T6	2.69	4.30	0.68	0.55	2.23	-1.72	1.87	0.38	-0.55	-6.31	-0.19	2.35	4.93	0.68	-5.11	4.70	-9.02	3.24	0.37
T7	3.57	6.70	1.63	4.72	0.47	-5.33	3.46	0.69	1.56	-5.33	0.50	3.42	5.69	0.17	-4.12	4.74	-8.04	4.64	-0.25
T8	2.21	5.06	0.06	3.87	2.50	-5.07	1.23	-0.99	-0.37	-6.51	-0.78	1.88	4.37	-0.16	-5.30	4.33	-0.52	2.74	-0.37
T9	2.86	4.29	0.76	0.26	2.23	-6.39	1.89	-0.46	-0.82	-6.39	-0.58	2.02	4.81	0.44	-5.18	4.70	-0.51	3.11	0.21
T10	3.06	6.47	1.48	5.29	1.17	-6.49	3.95	-0.44	2.00	-6.49	-0.42	2.17	4.53	-0.20	-5.28	4.17	-9.19	2.79	0.80

Table 5. Centered log ratio transformation of trace elements data of the basement rocks.

ID	Pb_clr	Zn_clr	Cu_clr	Li_clr	As_clr	B_clr	Ba_clr	Be_clr	Cd_clr	Co_clr	Cr_clr	Ga_clr	In_clr	Ni_clr	Sc_clr	Se_clr	Th_clr	U_clr	V_clr
D2b	2.39	3.93	0.60	-0.18	2.58	-2.06	0.35	-0.53	-0.60	-1.80	0.32	1.72	4.43	-0.11	-5.37	4.44	-2.55	2.83	-0.29
D24a	0.86	4.16	-0.35	-1.07	3.43	-3.58	-0.84	-1.35	-0.68	1.06	-0.45	1.44	1.87	0.59	-5.38	4.56	0.66	2.18	-0.02
D25a	3.76	8.20	3.75	7.82	-5.42	-5.42	3.30	0.95	4.65	-5.42	0.96	4.07	5.55	-5.42	-4.21	5.21	-8.13	4.22	0.28
S16	2.48	4.15	0.84	2.13	2.21	-6.63	4.20	-0.61	-0.31	-6.63	-0.75	2.27	4.70	0.08	-2.30	4.43	-9.34	2.89	0.97
K14	2.46	4.06	0.75	2.26	-6.23	-6.23	4.22	-0.43	-0.40	-6.23	1.46	2.18	4.79	0.55	-0.16	4.09	-8.93	2.98	2.84

K22	3.02	4.44	3.02	3.79	-6.07	-6.07	5.65	0.59	0.63	-6.07	4.35	2.82	5.29	2.16	1.07	2.38	-8.78	3.52	4.52
S13c	1.80	2.45	-0.23	-1.32	2.42	-0.92	0.03	-1.35	-1.43	0.21	-0.68	1.51	4.31	0.63	-5.58	4.47	-0.21	2.74	-0.16
S14	2.30	3.77	0.37	1.40	1.89	-1.06	1.59	-0.67	-1.03	-1.03	-0.52	1.79	4.56	0.37	-5.21	4.40	-9.12	2.91	-0.04
S26b	2.22	5.64	6.52	1.24	1.16	-3.05	3.22	-2.00	0.72	-1.56	-1.55	0.79	3.16	-1.15	-3.92	3.28	-1.46	1.84	-0.35
S28	4.55	5.46	1.59	4.52	-4.97	-4.97	4.80	0.91	1.49	-4.97	0.53	3.03	5.82	-4.97	-3.76	-6.57	-7.67	4.02	0.67
S29c	3.41	4.92	1.49	4.62	1.12	-6.57	1.78	-0.60	-0.03	-6.57	-0.64	2.14	4.72	0.10	-5.36	4.16	-9.28	2.90	-0.18

Table 6. Centred log-ratio transformation of subcompositions for examining Pb, Zn, Cu mineralization in the Saiya – Shokobo and Tongolo Complexes

SampleID	Fe_clr	Mn_clr	As_clr	Ba_clr	Cd_clr	Cu_clr	Pb_clr	Zn_clr
D1a	3.97	-0.14	0.26	0.26	-3.51	-2.26	0.27	1.16
D1b	4.11	0.50	-1.03	-0.12	-3.94	-1.92	0.56	1.84
D1c	5.16	0.30	-2.50	-2.21	-0.58	-1.74	-1.51	3.07
D12	4.41	0.48	-0.93	1.73	-3.61	-2.34	-0.56	0.82
D18	4.93	1.58	-3.99	-2.88	-2.42	-1.17	2.09	1.86
S1a	5.04	0.70	-8.08	2.45	-1.60	-1.25	0.59	2.15
S1c	5.10	1.56	-0.63	0.56	-3.82	-2.73	-0.67	0.63
S2a	4.42	0.72	0.01	0.18	-3.43	-1.80	-0.35	0.24
S2b	4.76	1.41	-1.46	-1.50	-3.17	-2.14	0.76	1.34
S6	5.64	2.18	-2.22	-0.56	-4.07	-1.20	-1.11	1.34
S15b	5.98	1.55	-8.09	-0.07	-1.91	-1.25	0.89	2.92
S17b	4.96	0.66	-0.73	0.00	-3.86	-1.24	-0.25	0.46
S7	4.83	1.34	-0.84	0.17	-3.58	-2.42	-0.45	0.96
S18	4.46	1.31	0.27	-1.07	-3.65	-2.22	-0.27	1.16
S19	4.31	0.90	-0.24	-1.06	-3.89	-0.61	-0.32	0.91
S20a	4.84	0.78	-0.21	-1.14	-3.85	-2.36	0.21	1.73
S21a	3.85	0.45	0.03	-1.37	-3.19	-1.96	-0.04	2.23
S22b	4.94	1.08	-2.23	-2.28	-1.41	-1.62	-1.29	2.81
S24c	5.84	1.77	-8.27	0.07	-1.55	-1.32	0.92	2.54
K1	4.66	0.67	-0.65	0.02	-3.26	-2.18	-0.24	0.98
S10	5.19	1.40	-0.44	0.40	-4.09	-2.31	-0.50	0.35
S11	5.81	1.77	-7.88	0.71	-1.50	-1.25	0.60	1.73
S12	4.41	0.13	0.14	-0.56	-3.98	-2.13	0.42	1.56
P10a	7.15	3.11	-8.81	-0.50	-1.93	-1.88	-0.15	3.01
P18b	5.13	1.54	-0.75	-1.11	-3.53	-2.30	-0.29	1.32
S13a	5.64	2.84	-3.84	-0.86	-2.75	-2.68	-0.75	2.39
S26c	4.71	0.80	-0.20	-1.46	-3.07	-2.64	-0.49	2.36
S29a	4.94	1.05	-0.63	-0.97	-3.68	-2.10	-0.01	1.42
S30	4.48	1.51	-2.85	-0.07	-2.02	-2.54	-0.97	2.45

Table 7. Centred log-ratio transformation of subcompositions for examining Pb, Zn, Cu mineralization in the basement rocks

SampleID	Fe_clr	Mn_clr	As_clr	Ba_clr	Cd_clr	Cu_clr	Pb_clr	Zn_clr
D2b	4.73	1.03	0.08	-2.16	-3.10	-1.90	-0.11	1.43

Science World Journal Vol. 21(No 2) 2026 https://dx.doi.org/10.4314/swj.v21i2.23
www.scienceworldjournal.org
ISSN: 1597-6343 (Online), ISSN: 2756-391X (Print)
Published by Faculty of Science, Kaduna State University

D24a	4.41	0.26	1.55	-2.71	-2.55	-2.23	-1.01	2.28
D25a	6.17	2.39	-9.89	-1.16	0.19	-0.72	-0.71	3.73
S16	5.07	1.58	-1.16	0.83	-3.68	-2.53	-0.89	0.77
K14	6.06	2.60	-8.48	1.97	-2.65	-1.51	0.21	1.81
K22	6.60	2.76	-9.41	2.31	-2.71	-0.32	-0.32	1.10
S13c	2.75	0.01	1.12	-1.27	-2.74	-1.53	0.50	1.15
S14	4.74	1.04	-0.56	-0.85	-3.48	-2.08	-0.15	1.32
S26b	2.59	-1.21	-2.31	-0.26	-2.75	3.04	-1.26	2.17
S28	7.05	4.84	-9.10	0.66	-2.65	-2.54	0.42	1.32
S29c	5.08	1.26	-2.05	-1.39	-3.20	-1.68	0.24	1.75

Figure 2. Biplots of the Principal Components analysis of Zn, Pb, Cu mineralization in (a) the Saiya – Shokobo and Tongolo Complexes (b) the basement rocks

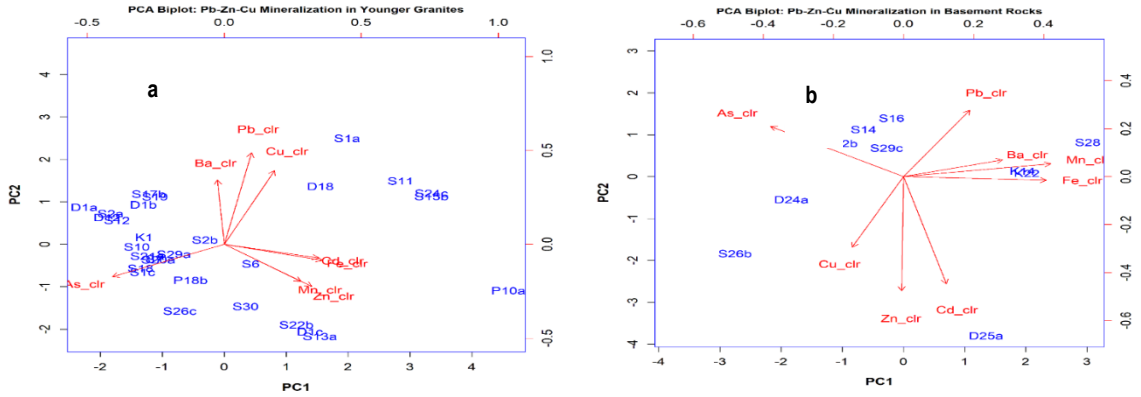

Table 8. PCA summary for Saiya – Shokobo & Tongolo complexes

Principal Component	Eigenvalue	Variance Explained (%)	Key Loadings
PC1	3.428	42.845	As(-0.51), Fe(+0.45), Cd(+0.43), Zn(+0.40)
PC2	1.392	17.395	Pb(+0.61), Cu(+0.49), Ba(+0.43)
PC3	1.310	16.377	Ba(-0.56), Mn(-0.45), Zn(+0.38), Fe(-0.37)
PC4	0.903	11.284	Ba(-0.60), Mn(+0.44), Cd(-0.42)
PC5	0.663	8.290	Cu(+0.73), Pb(-0.62)
PC6	0.165	2.058	Zn(+0.68), Cd(-0.68)
PC7	0.140	1.751	Fe(-0.76), Mn(+0.61)
PC8	0.000	0.000	As(+0.80)

Table 9. PCA summary for basement rocks

Principal Component	Eigenvalue	Variance Explained (%)	Key Loadings
PC1	3.393	42.416	Mn(+0.53), Fe(+0.51), As(-0.47)
PC2	2.440	30.497	Zn(-0.59), Cd(-0.56), Cu(-0.37), Pb(+0.35)
PC3	1.331	16.639	Ba(-0.62), Cu(-0.58)
PC4	0.602	7.524	Pb(-0.84)
PC5	0.136	1.705	Ba(+0.53), Cd(+0.52)
PC6	0.072	0.900	Zn(-0.65)
PC7	0.026	0.320	Mn(+0.64), Fe(-0.61)
PC8	0.000	0.000	As(+0.80)

Table 10. PC scores for Saiya – Shokobo & Tongolo complexes

Sample_ID	PC1	PC2	PC3	PC4	PC5	PC6	PC7	PC8
D1a	-2.25912	0.87275	0.616009	-0.86918	0.711239	0.034142	-0.17465	6.36E-08
D1b	-1.30123	0.932189	0.709976	-0.05531	0.699172	-0.80934	0.242714	-8.4E-08
D1c	1.383503	-2.05534	2.373713	-1.57919	-1.12163	0.496748	-0.63654	-5.9E-08
D12	-1.89274	0.632199	-1.19617	-1.52047	0.094271	-0.054	0.036315	-2.5E-08
D18	1.553064	1.367623	2.069547	2.456841	0.773676	0.647143	0.26904	-2.2E-08
S1a	1.980243	2.499658	-0.28415	-2.22781	0.095099	-0.17457	0.247407	4.66E-08
S1c	-1.31717	-0.65207	-1.9918	-0.12098	0.323222	0.336407	-0.06206	-1.3E-08
S2a	-1.8332	0.724836	-0.44934	-0.17218	-0.71954	0.673775	0.11796	-7.3E-08
S2b	-0.31064	0.106404	0.421033	1.18535	0.862577	0.497419	0.159716	-7.8E-08
S6	0.431135	-0.45944	-1.29339	1.090299	-1.93263	-0.75718	0.118673	-2.5E-08
S15b	3.344749	1.131753	0.286514	-0.07636	0.311901	-0.48847	-0.34167	4.21E-08
S17b	-1.2127	1.187278	-0.37307	0.348714	-1.38246	0.076922	-0.45133	-2E-09
S7	-1.12582	-0.34335	-1.10166	-0.1065	0.203449	0.200672	0.114029	-7.4E-08
S18	-1.34989	-0.56396	-0.02166	0.618799	0.103757	0.153229	0.368456	4.31E-08
S19	-1.11876	1.12333	0.843613	0.963812	-2.11919	-0.35161	0.492952	1.83E-08
S20a	-1.06147	-0.35907	0.367089	0.549328	0.800653	-0.34144	-0.51741	6.16E-08
S21a	-1.23858	-0.27494	1.772037	-0.17288	0.313208	-0.47653	0.454116	3E-08
S22b	1.166497	-1.88885	1.800666	-0.55362	-1.14191	0.17324	0.131381	6.77E-08
S24c	3.342169	1.205077	0.059369	-0.12395	0.349784	0.06863	0.011525	2.14E-08
K1	-1.2913	0.168653	-0.25899	-0.41165	0.05526	0.34982	-0.19723	8.04E-08
S10	-1.41114	-0.06019	-1.82305	0.310864	-0.20437	0.303835	-0.29051	3.48E-08
S11	2.845406	1.495822	-0.63654	-0.39663	-0.1972	0.607749	0.096179	1.61E-08
S12	-1.72968	0.564691	0.763416	0.043907	0.676241	-0.47354	-0.53037	-4.8E-08
P10a	4.586922	-1.08926	-1.61986	0.618902	0.194884	-0.33502	-0.42424	-9.7E-08
P18b	-0.54181	-0.84509	-0.47511	0.773253	0.174064	0.155159	-0.14762	1.12E-07
S13a	1.546875	-2.16484	-1.35297	0.445945	0.655167	-0.14463	0.584019	1.09E-07
S26c	-0.72052	-1.56584	0.791274	-0.23245	0.771856	-0.27763	-0.29487	-5.4E-09
S29a	-0.81039	-0.22983	0.029868	0.607372	0.193432	-0.10794	-0.31904	-4.8E-08

Science World Journal Vol. 21(No 2) 2026 https://dx.doi.org/10.4314/swj.v21i2.23
www.scienceworldjournal.org
ISSN: 1597-6343 (Online), ISSN: 2756-391X (Print)
Published by Faculty of Science, Kaduna State University

S30	0.345608	-1.46019	-0.02636	-1.39422	0.456032	0.017017	0.94305	-9.3E-08

Table 11. PC scores for basement rocks

Sample_ID	PC1	PC2	PC3	PC4	PC5	PC6	PC7	PC8
D2b	-0.95987	0.789845	0.892255	0.008527	-0.37908	0.195613	-0.14285	1.91E-08
D24a	-1.83433	-0.54941	1.25124	1.108401	0.000553	-0.09241	0.018184	5.74E-08
D25a	1.349006	-3.79449	1.196681	0.000258	0.251119	0.069806	-0.04272	-3E-08
S16	-0.19252	1.3971	-0.72187	1.431671	0.483405	0.060616	0.075989	-4.1E-08
K14	1.947694	0.134693	-0.62208	-0.46398	0.265723	-0.57542	0.068824	3.58E-08
K22	2.019392	0.081017	-1.663	0.151564	-0.04468	0.189204	-0.3287	1.66E-08
S13c	-1.66095	1.142475	0.517221	-1.45602	0.63404	0.233344	-0.01013	5.58E-09
S14	-0.6501	1.126535	0.282372	0.158931	-0.09416	-0.16996	-0.02104	-2.8E-08
S26b	-2.75368	-1.83678	-2.20662	-0.31761	-0.29258	0.057392	0.156427	-3.8E-10
S28	3.013223	0.821473	0.374613	-0.13616	-0.32777	0.339819	0.292082	1.02E-08
S29c	-0.27786	0.687537	0.699197	-0.48558	-0.49657	-0.30801	-0.06606	-4.6E-08

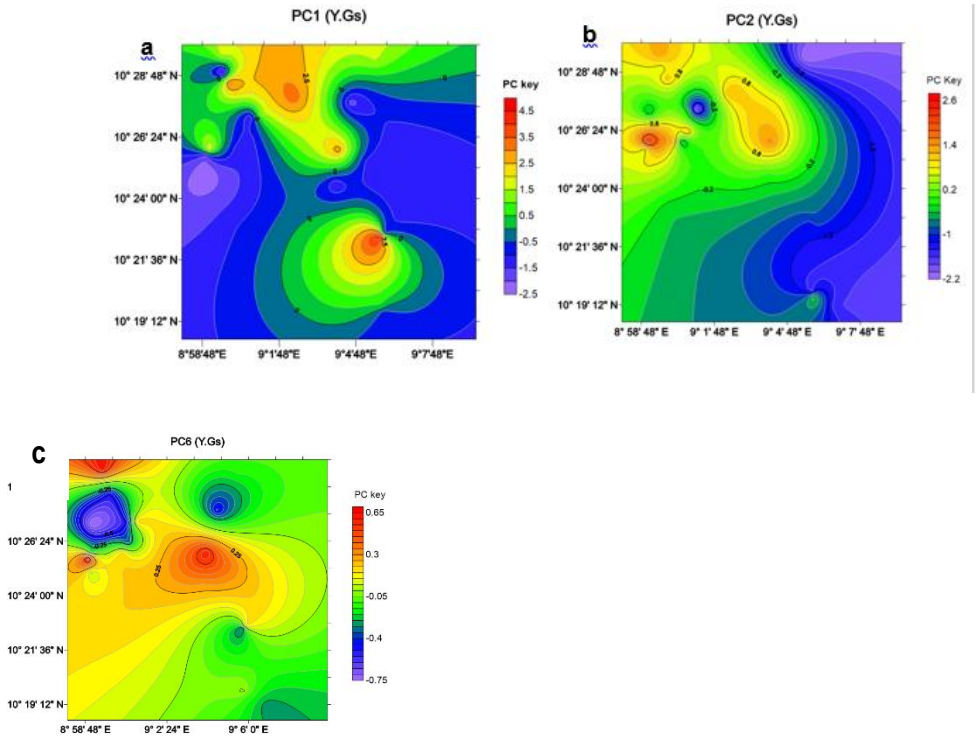

Figure 3. Geochemical plots based on PC scores of the Saiya – Shokobo and Tongolo complexes (a) PC1 (Fe-Zn-As Signature) (b) PC2 (Pb-Cu Association) (c) PC6 (Zn Specific)

Science World Journal Vol. 21(No 2) 2026 https://dx.doi.org/10.4314/swj.v21i2.23
www.scienceworldjournal.org
ISSN: 1597-6343 (Online), ISSN: 2756-391X (Print)
Published by Faculty of Science, Kaduna State University

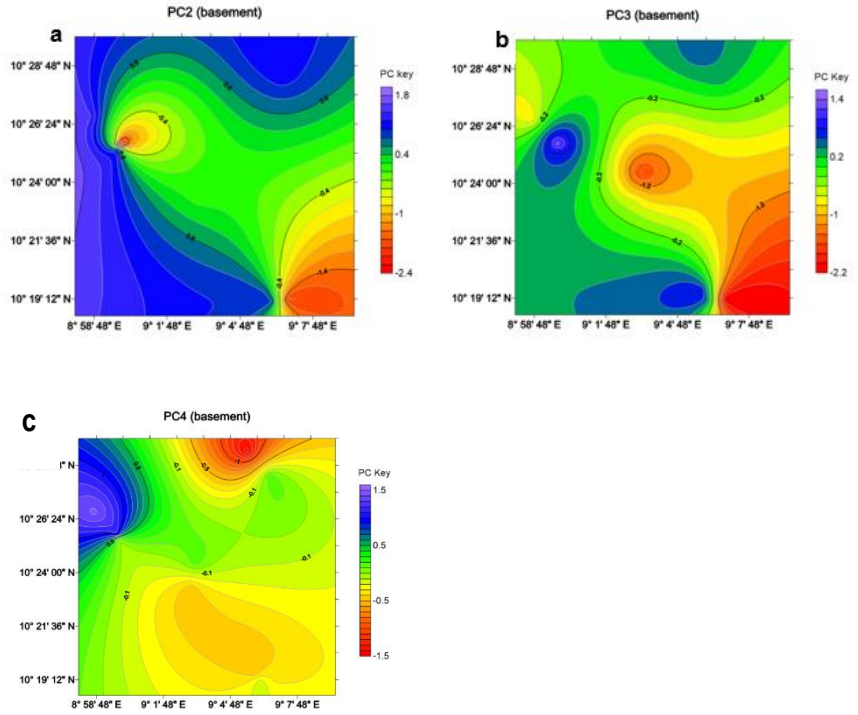

Figure 4. Geochemical plots based on PC scores of the basement rocks (a) PC2 (Zn-Cd-Cu association) (b) Lead (Pb) anomaly (c) Copper path

Structural features

The field structural features identified from geological mapping include joints, fractures, veins, and dykes. Figure 5 presents rose diagrams of structural measurements to illustrate the dominant orientation trends of these features and their relationship to mineralization pathways.

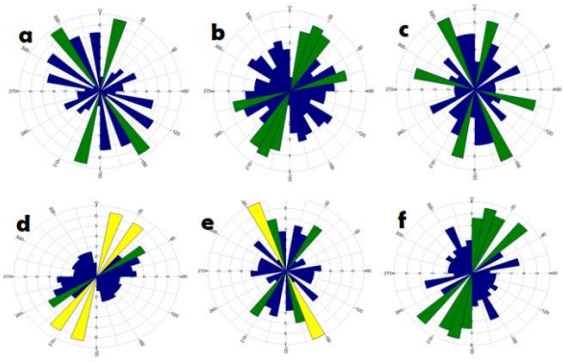

Figure 5. (a) Joints on rhyolites (major trend = NNE-SSW, NNW-SSE). (b) Joints on biotite granites (major trend = NNE-SSW, ENE-WSW). (c) Joints on porphyritic granites (major trend = NNW-SSE, NNE-SSW, WNW-ESE). (d) Joints on migmatites (major trend = NNE-SSW, NE-SW). (e) Quartzo-feldspathic veins on granite gneiss (major trend = NNW-SSE, NNE-SSW). (f) Quartzo-feldspathic veins on porphyritic granites (major trend = NNE-SSW, N-S, NE-SW)

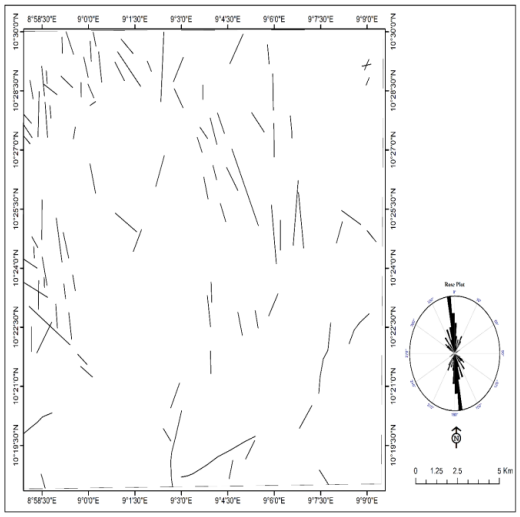

Figure 6. Lineaments map of study area showing major structural trends (NCRS Jos, 2023) Major Trend = N-S, NNW-SSE, minor trends = NW-SE, NE-SW

DISCUSSION

Structural analysis

The rocks of the study area have undergone tectonic deformation. The major trends of the structures found within the area are NNE-SSW, NNW-SSE, NE-SW, N-S (Fig. 5). These correlated with those reported by Kinnaird & Bowden (1987) and the major trends on the lineament map of the study area (Fig. 6). Kinnaird & Bowden

Science World Journal Vol. 21(No 2) 2026 https://dx.doi.org/10.4314/swj.v21i2.23
www.scienceworldjournal.org
ISSN: 1597-6343 (Online), ISSN: 2756-391X (Print)
Published by Faculty of Science, Kaduna State University

(1987) believed that the sites of the emplacement of the Nigerian Younger Granites and the mineralization that are associated with them are influenced by the NE-SW and NW-SE lineaments that originated from the reactivation of the Pan-African shear zones and transcurrent faults.

Geochemical Signatures of the Saiya-Shokobo and Tongolo Complexes.

The Kaiser Criterion suggested retaining three of the eight components - PC1, PC2, PC3 (with Eigenvalue >1) as significant components (Table 8, Fig. 2). PC1 represents (Fe-Zn-As Signature) with key loadings; As (-0.51), Fe (+0.45), Cd (+0.43), and Zn (+0.40). This component explains the most variance (42.8%). It links Zinc with Iron and Cadmium. It likely represents the broader hydrothermal "footprint" of the system. Because Arsenic (As) is negative (-0.51), high positive scores here represent areas high in Fe-Zn-Cd but low in As (Fig. 3a). PC2 represents (Pb-Cu Association) with key Loadings: Pb (+0.61), Cu (+0.49), Ba (+0.43). This Principal Component (PC) directly captures the Lead and Copper mineralization. Since both have positive loadings, high positive scores in geochemical map (Fig. 3b) point directly to the centers of Pb-Cu mineralization. However, we also examined components with lower eigenvalues to investigate other trace element associations. PC5 (λ = 0.66) also show a strong association between Cu and Pb, explaining 8.3% of the variance, while PC6 (λ = 0.17) isolates Zn and Cd and explains 2.1% of the variance. PC6 with key loadings: Zn (+0.68), Cd (-0.68) points to zinc-rich zones where Zinc is concentrated independently of Lead and Copper (Fig. 3c).

The PCA results (Table 8) for the Saiya-Shokobo and Tongolo complexes reveal a multi-stage or multi-process geochemical history for base metals within these felsic intrusions. While the Kaiser criterion (eigenvalue >1) retained the first three principal components as statistically dominant, explaining the majority of the dataset's variance, it is the components with lower eigenvalues that provide the most compelling evidence for discrete mineralization events (Jolliffe, 2002). This approach of examining minor but highly informative components is crucial in exploration geochemistry, where subtle but significant element associations can be masked by the variance associated with major rock-forming minerals (Grunsky, 2010). Therefore, the PC2 (λ = 1.39, 17.4% variance) and PC5 (λ = 0.66, 8.3% variance) components highlight a specific association between Cu and Pb, effectively decoupling them from the broader base-metal suite (e.g., Zn). In magmatic-hydrothermal systems, the transport and deposition of Cu and Pb are often controlled by the temperature, salinity, and composition of the ore-forming fluids (Seedorff *et al*., 2005). While Cu and Pb are traditionally separated by thermal zonation—with Cu typically sequestered in higher-temperature proximal zones and Pb in distal, lower-temperature settings—their statistical grouping here suggests a secondary control that transcends simple thermal gradients. This association likely represents temporal overprinting (telescoping), where Cu and Pb were precipitated in the same spatial domain at different stages of the system's evolution (Sillitoe, 2010). The spatial coincidence of Cu and Pb, as revealed by the multivariate mapping, suggests a shared structural plumbing system. This is consistent with the evolved nature of the Saiya-Shokobo complex, where initial high-temperature fluids were followed by cooler, Pb-rich pulses during the waning stages of the hydrothermal system (Olorunyomi *et al.,* in press). Such structural overprinting is a recognized phenomenon in evolved alkaline systems where pre-existing fracture networks act as long-lived conduits for successive mineralization events (Xu *et al*., 2023; Paoli *et al*., 2025).

The shared presence of these metals in PC2 and PC5 likely reflects the re-use of common conduits during successive mineralizing events. Specifically, the spatial overlap of a high-temperature Cu phase with a later, lower-temperature Pb overprint is consistent with the evolved nature of the system, as previously described by Pirajno (2009). Similar Cu-Pb assemblages have been documented in hydrothermal veins associated with alkaline ring complexes, such as those in the Nigerian Younger Granite province, where late-stage fluids are responsible for disseminating and vein-type mineralization (Kinnaird, 1985; Kinnaird & Bowden, 1987; Haruna, 2017; Amuda *et al*., 2022).

PC6 (λ = 0.17, 2.1% variance) isolates a very tight association between Zn and its pathfinder element, Cd. The near-perfect correlation of Zn and Cd is a classic geochemical signature, as Cd^{2+} substitutes readily for Zn^{2+} in sphalerite (ZnS). The substitution is driven by the fact that Cd and Zn belong to the same group in the periodic table (Group 12), leading to similar geochemical behavior. In the sphalerite crystal lattice, Zn is tetrahedrally coordinated by sulfur; Cd fits into these sites via simple isovalent substitution $Zn^{2+} \leftrightarrow Cd^{2+}$ (Cook *et al*., 2009; Li *et al*., 2022).The fact that this pair is isolated in a component of its own, distinct from the Cu-Pb association of PC5, is highly significant. It implies a separate and discrete mineralization event or physico-chemical condition that led to the preferential enrichment of Zn-Cd. This could represent a later, lower-temperature hydrothermal phase where Zn-dominated sulfides were deposited, separate from an earlier or higher-temperature Cu-Pb phase (Pirajno, 2009). The low variance explained by this component (2.1%) does not diminish its geological importance; rather, it suggests that this Zn-Cd mineralizing process was localized, subtle, or overprinted by the dominant rock-forming and alteration processes captured in the first three principal components. This finding aligns with observations in other peralkaline granite settings, where rare and highly fractionated, but economically significant, mineralized zones can be overlooked by bulk-rock analyses (Kinnaird & Bowden, 1987).

Geochemical Signatures of the Basement Rocks

As stated earlier, the Kaiser Criterion suggested retaining three of the eight components - PC1, PC2, PC3 (with Eigenvalue >1) as significant components (Table 9, Fig.2). PC2 represents (Zn-Cd-Cu Association) with key loadings: Zn (-0.59), Cd (-0.56), Cu (-0.37), Pb (+0.35). This points to multi-element mineralization. It captures the association between Zinc, Cadmium, and Copper. We observed that the loadings are negative. This means that on the geochemical map (Fig. 4a), the most negative values are the high-intensity anomalies. PC3 represents a possible copper path with key loading: Cu (-0.58). This captures an increase in copper concentrations which might represent a different style of mineralization. We also examined a component with lower eigenvalues to investigate lead (Pb) anomaly. PC4 (λ = 0.60) isolates Pb, explaining 7.5% of the variance and key loading: Pb (-0.84). we observe that in the basement rocks, Lead (Pb) seems to be behaving independently of the other metals (PC4 is almost

exclusively a "Lead component."). The geochemical map (Fig.4c) points to specifically targets for Galena (PbS) or lead-rich veins. Again, because the loading is negative (-0.84), the lowest/most negative scores (Table 11) are targets.

The PCA of the basement samples (Table 9) presents a different metallogenetic picture. As with the Younger Granites, the major components (PC1) likely represent the broad lithological variation of the porphyritic granites, gneisses, and migmatites. However, PC2, PC3 and PC4 provides critical insights as stated earlier. PC4 (λ = 0.60, 7.5% variance), which isolates Pb. The isolation of Pb from Zn and Cu in this component is also an indicator of its unique geochemical behaviour within the basement lithologies. This isolation can be interpreted in two primary, non-exclusive ways; First, it may point to the presence of discrete Pb-bearing minerals, such as K-feldspar, which can host significant lattice-bound Pb, or minerals like galena, within specific lithological units. During metamorphism and deformation, Pb can be mobilized and concentrated, but its geochemical cycle often differs from that of Zn and Cu, which are more chalcophile and associated with mafic minerals or sulfides (Doe, 1970; Robb, 2005; Cook *et al*., 2016; Fahmy *et al*., 2023). Second, and perhaps more importantly for exploration, this isolated Pb signature could represent a pre-concentration event within the basement that predates the intrusion of the Younger Granites. The basement complex of Nigeria is polymetamorphic and has experienced several orogenic cycles, which are known to have remobilized and concentrated base metals (Woakes *et al*.,1987; Adamu *et al*., 2024). The Pb isolated by PC4 may thus define a basement geochemical anomaly. From a metallogenic perspective, such a basement anomaly is highly significant as it could have acted as a source of metals for later hydrothermal systems, particularly those associated with the Younger Granite magmatism (Pirajno, 2009; Amuda *et al*., 2022). This concept of basement rocks as metal reservoirs is well-documented in other mineralized provinces, such as the relationship between Archean basement and Proterozoic unconformity-related uranium deposits in Canada and Australia (Jefferson *et al*., 2007; Richard *et al.,* 2015).

Implications for Mineralization Models.

Integrating the PCA results from both groups allows for the construction of a more comprehensive mineralization model for the study area. The data suggests a two-stage or dual-source model:

a. A Basement Metal Source: The basement rocks contain a discrete Pb signature (PC4), indicating a pre-existing enrichment or heterogeneous distribution of this metal. This could represent a regional background value or a specific metal-rich lithology. The lack of a strong Zn or Cu association in this component implies that these metals were either not pre-concentrated in the same manner or were mobilized differently during subsequent events.
b. A Magmatic-Hydrothermal Overprint: The intrusion of the Younger Granites complexes introduced a more complex hydrothermal system. The data from the granites record at least two distinct pulses: one carrying Cu-Pb (PC5) and a later, weaker, but highly specific Zn-Cd pulse (PC6). The Cu in the granites could be mantle-derived, a common feature in anorogenic magmatism, or leached from the country rock. Interestingly, the Pb in the granites' PC5 could have been partly scavenged from the Pb-rich basement as the highly reactive, mineralizing fluids circulated through the country rocks (Bowden, 1985; Emmermann, 1985; Adamu *et al*., 2024). The interaction of these metal-bearing magmatic fluids with the pre-enriched basement could have been the key mechanism for concentrating the observed polymetallic signatures, a process akin to that proposed for some intrusion-related gold deposits (Sillitoe & Thompson, 1998).

Summary

This research addresses the challenge of identifying multi-stage mineralization in the Saiya-Shokobo and Tongolo complexes by moving beyond univariate statistics to a Compositional Data Analysis (CoDA) framework. By applying the CLR transformation, the study successfully eliminated "spurious correlations" caused by the constant-sum constraint of geochemical data.

The findings indicate that mineralization was not a single event but a progression controlled by deep-seated structural lineaments. The study successfully differentiated between the "geochemical background" of the host rocks and the "geochemical signal" of the ore-forming fluids. Notably, the discovery of distinct metal associations in the basement (Pb-dominant) versus the granites (Cu-Pb and Zn-Cd pulses) provides a new temporal framework for the region. The use of PC-score mapping allowed for the spatial visualization of these distinct pulses, directly linking the geochemical anomalies to the NNE-SSW, NNW-SSE, NE-SW, N-S structural trends identified in the field.

Conclusion

The integration of structural geology and CLR-transformed multivariate statistics provides a robust methodology for deconstructing the polymetallic mineralization in the Nigerian Younger Granite Province. This work further affirms that application of CLR-PCA is superior to raw data analysis for lithogeochemical mapping, as it successfully isolates subtle mineralization stages (e.g., PC5 and PC6) that would otherwise be masked by the dominant lithological variance. Mineralization in the Saiya-Shokobo and Tongolo complexes is strictly controlled by the reactivation of Pan-African structural grains. The NE-SW and NW-SE fractures acted as the primary plumbing system for both the intrusion of the Younger Granites and the subsequent circulation of mineralizing fluids. The data supports a complex metallogenic history. We conclude that a pre-existing Pb enrichment existed within the basement rocks (PC4). The subsequent intrusion of the Younger Granites initiated a magmatic-hydrothermal system that both introduced new metals (Cu and Zn-Cd pulses) and potentially scavenged Pb from the pre-enriched basement. The identification of a Cu-Pb signature in the granites suggests a cooling hydrothermal system where metal deposition was partitioned over time within shared structural conduits. These insights not only refine the exploration model for North-Central Nigeria but also underscore the necessity of using CoDA-based workflows when interpreting geochemical data in complex tectonic settings.

REFERENCES

Adamu, L. M., Sunday, A. E., Ohiemi, A. F., Ayuba, R., Ugbena, K. G., Baba, Y., Abraham, T., Ogunkolu, B. A., & Ebeh, A. (2024). Petrogenesis and geochemical evolution of rocks and pegmatites in Kwarra area, Northcentral Nigeria: Implications for rare metal mineralization. *Economic and Environmental Geology*, *57*, 735–768.

Aga, T., & Haruna, A. I. (2019). The field geology and petrography of the Saiya-Shokobo Younger Granite Complex, Central Nigeria. *International Journal of Geology and Earth Science*, *5*, 25–45.

Aitchison, J. (1986). *The statistical analysis of compositional data*. Chapman and Hall.

Amuda, A. K., Li, S., Yang, X., Cao, J., & Faisal, M. (2022). Genetic association between granites and mineralization at the Gindi Akwati cassiterite–sulfide deposit, north-central Nigeria: Insights from mineralogy, fluid inclusions, and sulfur isotopes. *Minerals*, *12*, Article 761.

Andarawus, A., Abubakar, A. J., & others. (2023). Integrating remote sensing data with geochemical characteristics of Precambrian rocks from the Mambilla Plateau in northern Nigeria. *FUDMA Journal of Sciences*, *7*, 328–337.

Bailie, R. H., & Robb, L. J. (2004). Polymetallic mineralization in the granites of the Bushveld Complex – examples from the central southeastern lobe. *South African Journal of Geology*, *107*, 633–652.

Bestemianova, K. V., & Grinev, O. M. (2019). Geological structure and conditions of formation of Strizhkovskoe barite-polymetallic deposit (ore Altai). *IOP Conference Series: Earth and Environmental Science*, *319*, Article 012001.

Bowden, P. (1985). The geochemistry and mineralization of alkaline ring complexes: A review. *Journal of African Earth Sciences*, *3*, 17–39.

Cook, N. J., Ciobanu, C. L., George, L. L., Zhu, Z. Y., Wade, B. P., & Ehrig, K. (2016). Trace element analysis of minerals in magmatic-hydrothermal ores by laser ablation inductively-coupled plasma mass spectrometry: Approaches and opportunities. *Minerals*, *6*, Article 111.

Cook, N. J., Ciobanu, C. L., Pring, A., Skinner, W., Shimizu, M., Danyushevsky, L., Saini-Eidukat, B., & Melcher, F. (2009). Trace and minor elements in sphalerite: A LA-ICP-MS study. *Geochimica et Cosmochimica Acta*, *73*, 4761–4791.

Darabi-Golestan, F., & Hezarkhani, A. (2019). Applied statistical functions and multivariate analysis of geochemical composition data to evaluate mineralization in Glojeh polymetallic deposit, NW Iran. *Frontiers of Earth Science*, *13*, 229–246.

Doe, B. R. (1970). *Lead isotopes*. Springer-Verlag.

Du, G., Ling, X., Wang, D., Zhou, W., Yang, L., Lu, Y., & Zhang, Z. (2025). In-situ geochemical and sulfur isotopic composition of pyrites from the Jiepailing tin–beryllium polymetallic deposit, southern Hunan province, China: Implications for ore-forming processes. *Minerals*, *15*, Article 312.

Egozcue, J. J., Pawlowsky-Glahn, V., & Mateu-Figueras, G. (2003). Isometric logratio transformations for compositional data analysis. *Mathematical Geology*, *35*, 279–300.

Emmermann, R. (1985). Hydrothermal alteration of ocean-crust basalts. In J. Honnorez & R. P. Von Herzen (Eds.), *Initial Reports of the Deep Sea Drilling Project* (Vol. 83, pp. 83–95). U.S. Government Printing Office.

Erlandsson, V., Foltyn, K., Muchez, P., Rantitsch, G., Ellmies, R., & Melcher, F. (2025). Chalcopyrite, sphalerite, and pyrite chemistry in stratiform sediment-hosted Cu(-Co) metallogenic districts: Trace element characteristics and factors controlling polymetallic mineralization. *Mineralium Deposita*, *60*, 869–894.

Etschmann, B., Liu, W., Mayanovic, R., Mei, Y., Heald, S., Gordon, R., & Brugger, J. (2019). Zinc transport in hydrothermal fluids: On the roles of pressure and sulfur vs. chlorine complexing. *American Mineralogist*, *104*, 158–161.

Fahmy, W., El-Desoky, H. M., Elyaseer, M. H., Ayonta Kenne, P., Shirazi, A., Hezarkhani, A., Shirazy, A., El-Awny, H., Abdel-Rahman, A. M., Khalil, A. E., Eraky, A., & Pour, A. B. (2023). Remote sensing, petrological and geochemical data for lithological mapping in Wadi Kid, Southeast Sinai, Egypt. *Minerals*, *13*, Article 1160.

Filzmoser, P., Hron, K., & Reimann, C. (2009). Univariate statistical analysis of environmental (compositional) data: Problems and possibilities. *Science of the Total Environment*, *407*, 6100–6108.

Filzmoser, P., Hron, K., & Reimann, C. (2010). The bivariate statistical analysis of environmental (compositional) data. *Science of the Total Environment*, *408*, 4230–4238.

Grunsky, E. C. (2010). The interpretation of geochemical survey data. *Geochemistry: Exploration, Environment, Analysis*, *10*, 27–74.

Grunsky, E. C., & Smee, B. W. (1999). The differentiation of soil types and mineralization from multi-element geochemistry using multivariate methods and digital topography. *Journal of Geochemical Exploration*, *67*, 287–299.

Grunsky, E. C., & de Caritat, P. (2020). State-of-the-art analysis of geochemical data for mineral exploration. *Geochemistry: Exploration, Environment, Analysis*, *20*, 217–232.

Grunsky, E. C., Mueller, U. A., & Corrigan, D. (2014). A study of the lake sediment geochemistry of the Melville Peninsula using multivariate methods: Applications for predictive geological mapping. *Journal of Geochemical Exploration*, *141*, 15–41.

Haruna, I. V. (2017). A review of the geology and mineralization of the Nigerian Younger Granite Province. *Journal of Applied Geology and Geophysics*, *5*, 52–60.

Imeokparia, E. G. (1985). Geochemistry of the younger granites of Guinea: A comparative study with the Nigerian younger granite province. *Journal of African Earth Sciences*, *3*, 153–159.

Jefferson, C. W., Thomas, D. J., Gandhi, S. S., Ramaekers, P., Delaney, G., Brisbin, D., Cutts, C., Portella, P., & Olson, R. A. (2007). Unconformity-associated uranium deposits of the Athabasca Basin, Saskatchewan and Alberta. In W. D. Goodfellow (Ed.), *Mineral Deposits of Canada: A Synthesis of Major Deposit-Types, District*

Metallogeny, the Evolution of Geological Provinces, and Exploration Methods (Vol. 5, pp. 273–305). Geological Association of Canada.

Jolliffe, I. T. (2002). *Principal component analysis* (2nd ed.). Springer.

Jolliffe, I. T., & Cadima, J. (2016). Principal component analysis: A review and recent developments. *Philosophical Transactions of the Royal Society A*, *374*, Article 20150202.

Kinnaird, J. A. (1985). Hydrothermal alteration and mineralization of the alkaline anorogenic ring complexes of Nigeria. *Journal of African Earth Sciences*, *3*, 229–251.

Kinnaird, J. A., & Bowden, P. (1987). African anorogenic alkaline magmatism and mineralization — A discussion with reference to the Niger-Nigeria Province. *Geological Journal*, *22*, 297–340.

Li, L., Han, R., Zhang, Y., Wu, J., & Feng, Z. (2022). Trace element signatures of sphalerite in the Sichuan Daliangzi Ge-rich Pb-Zn deposit and its implications for deep ore prospecting. *Frontiers in Earth Science*, *10*, Article 981442.

Li, Y., Wang, J., Wei, S., Hu, J., Wang, Z., & Ge, J. (2024). Granites of the Chazangcuo copper-lead-zinc mining area in Tibet, China: Magma source and tectonic implications. *Minerals*, *14*, Article 1227.

Obaje, N. G. (2009). *Geology and mineral resources of Nigeria*. Springer-Verlag.

Olorunyomi, A. E., Olobaniyi, S. B., & Odukoya, A. M. (in press). Petrographic and ore microscopy analysis of lead–zinc–copper–lithium mineralization in the Saiya–Shokobo, Tongolo Complexes and intruded basement rocks: Implications for host rock selection and metallogenesis. *Journal of Mining and Geology*.

Oyebamiji, A., Adewumi, A. J., Zafar, T., Odebunmi, A., Falae, P., & Fadamoro, O. (2018). Petrogenetic and compositional features of rare metal Pan-African post-collisional pegmatites of southwestern Nigeria: A status review. *Contemporary Trends in Geoscience*, *7*, 166–187.

Paoli, G., Dini, A., Vezzoni, S., Ovtcharova, M., & Rocchi, S. (2025). Asynchronous transfer of magmas and mineralizing fluids in a plutonic-subvolcanic-volcanic plumbing system. *Scientific Reports*, *15*, Article 4321.

Pirajno, F. (2009). *Hydrothermal processes and mineral systems*. Springer.

Reimann, C., Filzmoser, P., Fabian, K., Hron, K., Birke, M., Demetriades, A., Dinelli, E., & Ladenberger, A. (2012). The concept of compositional data analysis in practice – total major element concentrations in agricultural and grazing land soils of Europe. *Science of the Total Environment*, *426*, 196–210.

Reimann, C., Filzmoser, P., Hron, K., Kynclova, P., & Garrett, R. G. (2017). A new method for correlation analysis of compositional (environmental) data – a worked example. *Science of the Total Environment*, *607–608*, 965–971.

Richard, A., Cathelineau, M., Boiron, M.-C., Mercadier, J., Banks, D.A., & Cuney, M. (2015). Metal-rich fluid inclusions provide new insights into unconformity-related U deposits (Athabasca Basin and Basement, Canada). *Mineralium Deposita*, *51*, 249–270.

Robb, L. (2005). *Introduction to ore-forming processes*. Blackwell Publishing.

Seedorff, E., Dilles, J. H., Proffett, J. M., Einaudi, M. T., Zurcher, L., Stavast, W. J. A., & Barton, M. D. (2005). Porphyry deposits: Characteristics and origin of hypogene features. In J. W. Hedenquist, J. F. H. Thompson, R. J. Goldfarb, & J. P. Richards (Eds.), *Economic Geology 100th Anniversary Volume* (pp. 251–298). Society of Economic Geologists.

Seyedrahimi-Niaraq, M., & Mahdiyanfar, H. (2025). Analysis of closed and open numerical systems of geochemical data in spatial statistics environment in order to separate anomalous areas. *Scientific Reports*, *15*, Article 21254.

Sillitoe, R. H. (2010). Porphyry copper systems. *Economic Geology*, *105*, 3–41.

Sillitoe, R. H., & Thompson, J. F.H. (1998). Intrusion-related vein gold deposits: Types, tectono-magmatic settings and difficulties of distinction from orogenic gold deposits. *SGA News*, *6*, 10–15.

Solomon, A. O. (2005). *A study of natural radiation levels and distribution of dose rates within the Younger Granite Province of Nigeria* (Doctoral dissertation, University of Jos).

Wang, J., Zuo, R., & Liu, Q. (2024). Mapping geochemical anomalies by accounting for the uncertainty of mineralization-related elemental associations. *Solid Earth*, *15*, 731–746.

Wang, L., Liu, B., McKinley, J. M., Cooper, M. R., Li, C., Kong, Y., & Shan, M. (2021). Compositional data analysis of regional geochemical data in the Lhasa area of Tibet, China. *Applied Geochemistry*, *135*, Article 105108.

Watts, M. J., Middleton, D. R. S., Marriott, A. L., Humphrey, O. S., Hamilton, E. M., Gardner, A., Smith, M., McCormack, V. A., Menya, D., Munishi, M. O., Mmbaga, B. T., & Osano, D. (2019). Source apportionment of micronutrients in the diets of Kilimanjaro, Tanzania and Counties of Western Kenya. *Scientific Reports*, *9*, Article 14447.

Woakes, M., Rahaman, M. A., & Ajibade, A. C. (1987). Some metallogenetic features of the Nigerian basement. *Journal of African Earth Sciences*, *6*, 655–664.

Xu, Y., Wang, G., Gao, M., Yang, W., Yang, S., Yun, H., Wu, P., Guo, N., & Feng, Y. (2023). Genesis of the Shibaogou Mo–Pb–Zn deposit in the Luanchuan ore district, China: Constraints from geochronology, fluid inclusion, and H–O–S–Pb isotopes. *Frontiers in Earth Science*, *10*, Article 1096338.

Yan, Q.-H., Chi, G., Wang, H., Liu, B., & Zhang, W. (2024). Formation of a granite-related Sn-Pb-Zn-(Ag) deposit from three discrete mineralization events around a common magmatic-hydrothermal centre over a span of ~45 million years at Changpu, eastern Guangdong, South China. *Economic Geology*, *120*, Article 105231.

Yang, L., Liu, Z., Li, Z., Ouyang, Y., Chen, Q., Du, B., Zhang, R., Zhang, H., Luo, C., & Guo, J. (2025). The Lengshuikeng porphyry type Ag-Pb-Zn-Cd deposit: Insights from magmatism–mineralization timing sequence, chemical composition and in-situ Pb isotope of sulfide. *Ore Geology Reviews*, *177*, Article 106460.

Zuo, R. (2011). Identifying geochemical anomalies associated with Cu and Pb-Zn skarn mineralization using principal component analysis and spectrum–area fractal modeling in the Gangdese Belt, Tibet (China). *Journal of Geochemical Exploration*, *111*, 13–22.

Zuo, R., Xia, Q., & Wang, H. (2013). Compositional data analysis in the study of integrated geochemical anomalies associated with mineralization. *Applied Geochemistry*, *28*, 202–211.